Nat. Hazards Earth Syst. Sci. Discuss., 3, 5297–5323, 2015
www.nat-hazards-earth-syst-sci-discuss.net/3/5297/2015/
doi:10.5194/nhessd-3-5297-2015

Natural Hazards and Earth System Sciences
Open Access
Discussions

Strong ground motion prediction for southwestern China from small earthquake records

Z. R. Tao[1], X. X. Tao[2], and A. P. Cui[1]

[1]Key Laboratory of Earthquake Engineering and Engineering Vibration, Institute of Engineering Mechanics, China Earthquake Administration, Harbin, China
[2]Harbin Institute of Technology, Harbin, China

Received: 9 July 2015 – Accepted: 11 August 2015 – Published: 4 September 2015

Correspondence to: Z. R. Tao (taozhengru@aliyun.com)

Published by Copernicus Publications on behalf of the European Geosciences Union.

Abstract

For regions lack of strong ground motion records, a method is developed to predict strong ground motion by small earthquake records from local broadband digital earthquake networks. Sichuan and Yunnan regions, located in southwestern China, are selected as the targets. Five regional source and crustal medium parameters are inversed by micro-Genetic Algorithm. These parameters are adopted to predict strong ground motion for moment magnitude (M_w) 5.0, 6.0 and 7.0. Strong ground motion data are compared with the results, most of the result pass through ideally the data point plexus, except the case of M_w 7.0 in Sichuan region, which shows an obvious slow attenuation. For further application, this result is adopted in probability seismic hazard assessment (PSHA) and near-field strong ground motion synthesis of the Wenchuan Earthquake.

1 Introduction

Ground motion prediction equation (GMPE) is a vital field in the research of engineering seismology. A great number of research results have been reported. At the time of this writing, most of achievements are empirical, such as Next Generation Attenuation (NGA) project in US and some studies in Japan (Si and Midorikawa, 2000; Kanno, 2006). This kind of empirical methods are based on plenty of observed strong ground motion data, so strictly speaking, it is only efficient for the regions like western US and Japan. For the regions without enough strong motion data for regression, like China, it is difficult to predict strong ground motion by these methods. The main focus of this study is to develop a method for strong ground motion prediction in these regions. Small earthquake data, recorded by the regional earthquake networks, rather than strong motion networks, are adopted in our method. Since the occurrence frequency of small earthquakes are higher than large ones, and digital earthquake networks record in real time, small earthquake data are much richer than strong motion data. The restriction of strong ground motion records insufficient in the empirical methods will be overcome

NHESSD
3, 5297–5323, 2015

effectively, if it is accurate to estimate acceleration Fourier spectra by velocity time histories of small earthquake data. The pioneer work can be traced to the stochastic simulation of strong ground motion, started at the beginning of 1980s (Hanks and McGuire, 1981; Boore, 1983; Aktinson, 1984; Boore and Atkinson, 1987).

Five regional source and crustal medium parameters, stress drop $\Delta\sigma$, quality factor Q_0 and η, geometric factor R_1 and R_2, are inversed by micro-Genetic Algorithm. Envelops of Fourier spectra from small earthquake data are the objective function. The models of source and wave propagation are based on digital observation data, so the physical mechanism is clear. The seismicity in Sichuan and Yunnan regions is the most active in China. We report here for the first time, strong ground motion is predicted for both regions, and is compared with strong ground motion data to prove the feasibility of this method.

An engineering site in Sichuan region is an example to illustrate the application in PSHA. And, these five inversed parameters are taken into hybrid source models. Near-field strong ground motion is synthesized and compared with the records in the Wenchuan Earthquake at two rock stations.

2 Database

2.1 Small earthquake records from local broadband digital earthquake networks

Sichuan digital earthquake network operated from December of 2000, and Yunnan digital earthquake network operated from August of 1999, so small earthquake data used here is from January of 2001 to December of 2007. There are 29 digital seismological stations in Sichuan and 26 stations in Yunnan, till 2007, the locations are shown in Fig. 1.

NHESSD
3, 5297–5323, 2015

In Sichuan, 147 records from 82 small earthquakes ($M_w = 3.5 \sim 4.5$, focal depth $\leq$ 30 km), recorded by these stations, are collected and processed; 863 records from 154 small earthquakes are in Yunnan. The distribution of epicenter is shown in Fig. 2.

The distributions of focal depth and hypocentral distance with M_w are shown in Figs. 3 and 4.

In both regions, the hypocentral distance is distributed uniformly from 50 to 300 km.

These velocity time histories, with time interval 0.02 s, are truncated from the time of S wave arrive to that of 80 % energy included for the following steps.

2.2 Strong ground motion records from China Strong Motion Networks Center

In the target regions, there are 69 strong ground motion stations in Sichuan and 36 stations in Yunnan; 1234 records from 118 Sichuan earthquakes ($M_w \geq 4.5$, focal depth $\leq$ 30 km) are collected, which are all from the aftershocks of Wenchuan Earthquake; 78 records from 27 Yunnan earthquakes. The distributions of M_w-focal depth and M_w-hypocentral distance are shown in Figs. 5 and 6.

Focal depth is from 8 to 20 km in Sichuan region, and most focal depths of big earthquakes in Yunnan province are less than 15 km.

Hypocentral distance is distributed uniformly from 50 to 300 km in Sichuan region, and most hypocentral distances are less than 120 km in Yunnan region, some are less than 20 km.

3 Methodology

Assuming that the far-field accelerations on an elastic half space are band-limited, finite-duration and white Gaussian noise, and the approach is based on Brune ω^2

NHESSD
3, 5297–5323, 2015

source spectrum (Boore, 2003), the Fourier spectrum on a site can be presented as:

$$\mathrm{FA}(M_0,f,R)=\frac{R_{\theta\varphi}FV}{4\pi R_0\rho_s\beta_s^3}\times\frac{M_0}{\left[1+\left(\frac{f}{f_0}\right)^a\right]^b}\times\exp\left[-\frac{\pi fR}{Q(f)\beta_s}\right]\times\left[1+\left(\frac{f}{f_{\max}}\right)^8\right]^{-1/2}\times(2\pi f)^z\times G(R)\times A(f) \quad (1)$$

where, $R_{\theta\varphi}$ is the radiation pattern of the shear excitation, with the assumption that the energy was equally partitioned into two horizontal components, $R_{\theta\varphi}=0.6$; F is the free surface effect, $F=2.0$; V is the vectorial partitioning of shear wave energy into two components of equal amplitude, $V=\frac{1}{\sqrt{2}}$; R_0 is a reference distance, $R_0=1\,\mathrm{km}$; ρ_s is the density in the vicinity of the source, $\rho_s=2.8\,\mathrm{g\,cm^{-3}}$; β_s is the shear-wave velocity in the vicinity of the source; M_0 is the seismic moment, $\beta_s=3.5\,\mathrm{km\,s^{-1}}$ (Wu et al., 2001; Xie et al., 2012); f is the frequency; f_0 is the corner frequency, $f_0=4.9\times10^6\times\beta_s\times(\Delta\sigma/M_0)^{1/3}$, $\Delta\sigma$ is the stress drop; $a=3.05$–$3.33\,\mathrm{M}$, $b=2.0/a$ (Wang, 2001); $f_{\max}$ is the high-frequency cutoff frequency; z is the index variable, $z=0$, 1 and 2 is for displacement, velocity and acceleration; R is the hypocentral distance; $Q(f)$ is the quality factor, $Q(f)=Q_0f^\eta$; $G(R)$ is the geometric spreading function, tri-linear model (Atkinson and Mereu, 1992; Atkinson and Boore, 1995) is adopted; $A(f)$ is the amplification factor of near surface amplitude as a function of hypocentral distance R and frequency f.

Stress drop $\Delta\sigma$ is one of the fundamental properties of the slip geometry of an earthquake, and the relation with the size of earthquake is currently under study. For large and shallow earthquakes, $\Delta\sigma$ varies from about 1 to 10 MPa (Shearer, 2009). In some researches, $\Delta\sigma$ is set as 8 MPa (Atkinson and Silva, 2000). Q is the frequency-dependent quality factor of shear waves, which describes the energy loss from anelastic processes or internal friction during wave propagation. Geometric spreading depends on the geometry of spreading in a layered crust apparently. Since stress drop

NHESSD
3, 5297–5323, 2015

$\Delta\sigma$, quality factor Q_0 and η, geometric spreading factor R_1 and R_2 describe the characteristics of regional source and crustal medium and are difficult to be measured directly. So, these parameters are inversed by micro-Genetic Algorithm (μGA), since they are considered as unrelated with the size of earthquakes on an interested frequency band.

These inversed parameters are taken into Eq. (1) to obtain Fourier amplitude spectra from generation j as objective spectra FA_j and Fourier amplitude spectra of small earthquake records are enveloped as FA_0. The objective function is the least-square residual between the enveloped Fourier spectra and the objective spectra, which is:

$$\varphi_j = \sum_{i=1}^{4096} \sum_{k=1}^{N} [FA_0(i,k) - FA_j(i,k)]^2 \quad (2)$$

where, i is the points on a Fourier spectrum; k is observed records; N is the number of small earthquake records.

In this inversion, the ranges of inverse parameters are determined by researches of some seismologists (Atkinson and Boore, 1995; Qiao et al., 2006; Mao et al., 2005; Zhang et al., 2007; Qin and Kan, 1986; Su et al., 2006; Liu, 2005; Hu et al., 2003), the optimum solution, after searching among 2000 generations, are listed in Table 1.

Fourier amplitude spectrum is combined with random phase spectrum, the complex Fourier spectrum can be transformed into time domain. In time-domain simulations (Boore, 2003), the time series is windowed by:

$$f(t) = \begin{cases} (t/t_1)^2, & 0 \le t \le t_1 \\ 1.0, & t_1 < t \le t_2 \\ \exp[-c\,(t - t_2)], & t_2 < t \end{cases} \quad (3)$$

NHESSD
3, 5297–5323, 2015

where, t_1 and t_2 are the starting point and finishing point of the stable section, c is the attenuation rate. Here, the envelop curve on bedrock is adopted (Huo and Hu, 1991):

$$\begin{cases} \log_{10} t_1 = -1.074 + 1.005 \times \log_{10}(R+10) \\ \log_{10} t_2 = -2.268 + 0.3262 \times M_w + 0.5815 \times \log_{10}(R+10) \\ \log_{10} c = 1.941 - 0.2817 \times M_w - 0.5870 \times \log_{10}(R+10) \end{cases} \quad (4)$$

The windowed time history is transformed into frequency domain, and the real and the imaginary parts are normalized by the modulus. Then, the complex spectrum is transformed back to time domain, and PGA for a magnitude-hypocentral distance pair can be picked. To reduce the effect of randomicity, 50 acceleration time histories are synthesized and the average PGAs are obtained.

4 Results and discussion

4.1 Strong ground motion prediction in Sichuan and Yunnan regions

Observed strong ground motion data, mentioned in Sect. 2.2, are adopted for comparison, which with $M_w \pm 0.5$ are for the attenuation curve of M_w, as shown in Fig. 7.

As shown in figure, in the cases of $M_w = 5.0$ and $M_w = 6.0$, our results pass through strong ground motion data, and the data points are distributed relatively uniform on two sides of up and down. It means our results can present the mean ground motion levels. In the case of $M_w = 7.0$, our result for Sichuan region is higher than the observed data from an earthquake with M_w 6.5.

Residual between the observed value and the predicted value is calculated by Eq. (5) and shown in Fig. 8.

$$\varepsilon = \log_{10}\left(\frac{\mathrm{PGA}}{\mathrm{PGA}'}\right) = \log_{10}\mathrm{PGA} - \log_{10}\mathrm{PGA}' \quad (5)$$

NHESSD
3, 5297–5323, 2015

where, PGA is the observed PGA, PGA′ is the predicted PGA.

In the case of M_w 5.0 and M_w 6.0, which means the ratios of the observed values and the predicted values are around 1. The discreteness of residuals decreases with the hypocentral distance. The residuals of M_w 7.0 in Sichuan region are lower than 0.

To describe the statistical characterization quantificationally, the mean value μ and the standard deviation σ are calculated by:

$$\mu = \frac{1}{N}\sum_{i=1}^{N}\varepsilon_i \tag{6}$$

$$\sigma = \sqrt{\frac{1}{N}\sum_{i=1}^{N}(\varepsilon_i - \mu)^2} \tag{7}$$

where, N is the number of observed strong ground motion records, ε_i is the residual from Eq. (5). The values are listed in Table 2.

As shown in Table 2, this result is close to the observed strong ground motion data, however, in this study, we use small earthquake data, recorded by regional broadband earthquake networks, rather than strong ground motion records.

4.2 Application in near-field ground motion synthesis

Near-field ground motion is complicated and related with the source mechanism, which is the limitation of GMPEs. However, the five inversed regional parameters of this study are necessary for near-field ground motion synthesis. Two rock-site stations, Maoxian station (103.9° E, 31.7° N) and Pixian station (103.7° E, 30.9° N), are examples. They are in the areas of intensity IX and VIII during the Wenchuan Earthquake, respectively.

These inversed parameters are taken into a finite fault model (Sun, 2010), and 30 hybrid source models are synthesized, 10 of them are shown in Fig. 9.

For each station, 30 acceleration time histories are synthesized from these 30 models, the mean values of PGAs are listed in Table 3.

NHESSD
3, 5297–5323, 2015

Synthesized PGAs in Table 3 disperse around the mean values. It shows the randomness of ground motion. However, the mean values are close to the observed PGAs. Response spectra of these time histories are shown as gray lines in Fig. 10, in which the black dot line is the mean spectra of 30 models, the black solid line is from Model 4.

So Model 4, represented the average characteristic, is adopted to synthesize acceleration time histories, shown as the top two in Fig. 11. The middle twos are observed time histories on EW direction, and the bottom twos are the observation on NS direction.

It is seen in Fig. 11 that the amplitudes are close; however, the durations are different obviously. For Maoxian station, the second and the third shocks are not synthesized. And, we compare the response spectra from Model 4 and observed time histories, shown as the black solid line and dot lines in Fig. 12.

At Maoxian station, the spectra are close to each other, however, they are different during 0.3–0.4 s and around 0.2–0.4 s at Pixian station.

5 Conclusions

Strong ground motion is predicted by small earthquake data, recorded by broadband digital earthquake networks, for southwestern China. Envelops of Fourier spectra of these small earthquake records are used to inverse five regional parameters, which are the keys to synthesize acceleration time histories. By comparing strong ground motion data, the feasibility of this method is proved. It is effective for the regions lack of strong ground motion data. And, these five parameters are adopted in the near-field strong ground motion synthesis of finite fault hybrid source models at two rock stations in Sichuan. The synthesized time histories and response spectra are compared with the observed ones during the Wenchuan Earthquake. The amplitudes of time histories are close, the durations are different. However, the response spectra from Model 4 are close with the observed ones.

NHESSD
3, 5297–5323, 2015

Data and resources

Small earthquake data, recorded by local broadband digital earthquake networks, were directly download from China Earthquake Networks Center (http://www.csndmc.ac.cn/newweb/index.jsp, last accessed June 2011). Strong ground motion records were directly download from China Strong Motion Networks Center (http://www.csmnc.net/, last accessed June 2012). The program of μGA, used to inverse the regional parameter, is developed from Carroll, D. L. (http://cuaerospace.com/carroll/ga.html, last accessed 20 November 2009).

Acknowledgements. This work was financially supported by National Nature Science Foundation of China 51178435, 51478443 and 51178151 and International Science and Technology Cooperation Program of China 2011DFA21460.

References

Atkinson, G. M.: Attenuation of strong ground motion in Canada from a random vibrations approach, B. Seismol. Soc. Am., 74, 2629–2653, 1984.

Atkinson, G. M. and Boore, D. M.: Ground-motion relation for Eastern North America, B. Seismol. Soc. Am., 85, 17–30, 1995.

Atkinson, G. M. and Mereu, R. F.: The shape of ground motion attenuation curves in Southeastern Canada, B. Seismol. Soc. Am., 82, 2014–2031, 1992.

Atkinson, G. M. and Silva, W.: Stochastic modeling of California ground motions, B. Seismol. Soc. Am., 90, 255–274, 2000.

Boore, D. M.: Stochastic simulation of high-frequency ground motions based on seismological models of the radiated spectra, B. Seismol. Soc. Am., 73, 1865–1894, 1983.

Boore, D. M.: Simulation of ground motion using the stochastic method, Pure Appl. Geophys., 160, 635–676, 2003.

Boore, D. M. and Atkinson, G. M.: Stochastic prediction of ground motion and spectral response parameters at hard-rock sites in Eastern North America, B. Seismol. Soc. Am., 77, 440–467, 1987.

NHESSD

3, 5297–5323, 2015

Hanks, T. C. and McGuire, R. K.: The character of high frequency strong ground motion, B. Seismol. Soc. Am., 71, 2071–2095, 1981.
Hu, J. F., Cong, L. L., Su, Y. J., and Kang, G. F.: Distribution characteristics of *Q* value of the *Lg* coda in Yunnan and its adjacent regions, Chinese J. Geophys.-Ch., 46, 809–813, 2003.
Huo, J. R. and Hu, Y. X.: Study on envelop function of acceleration time history, Earthq. Eng. Eng. Vib., 11, 1–12, 1991.
Kanno, T., Narita, A., Morikawa, N., Fujiwara, H., and Fukushima, Y.: A new attenuation relation for strong ground motion in Japan based on recorded data, B. Seismol. Soc. Am., 96, 879–897, 2006.
Liu, C.: Attenuation of strong ground motion from random vibration method, Master Dissertation, Harbin Institute of Technology, Harbin, China, 67 pp., 2005.
Mao, Y., Xu, Y., Wang, B., Hu, J. F., and Cong, L. L.: Distribution characteristics of the value *Q* of Lg coda in Sichuan and its adjacent regions, J. Seism. Res., 28, 38–42, 2005.
Qiao, H. Z., Zhang, Y. J., Zheng, W. Z., and Liu, J.: The inversion of the inelastic coefficient of the medium in North-West of Sichuan province, Seism. Geomagn. Obs. Res., 27, 1–7, 2006.
Qin, J. Z. and Kan, R. J.: *Q* values and seismic moments estimates using the coda waves of near earthquakes in the Kunming and surrounding regions, ACTA Geophys. Sinica, 29, 145–156, 1986.
Shearer, P. M.: Introduction to Seismology, 2nd edn., Cambridge University Press, London, 2009.
Si, H. J. and Midorikawa, S.: New attenuation relations for peak ground acceleration and velocity considering effects of fault type and site condition, in: Proc. of 12th World Conference on Earthquake Engineering, , Auckland New Zealand, 30 January–4 February, No. 0532, 2000.
Su, Y. J., Liu, J., Zheng, S. H., Liu, L. F., Fu, H., and Xu, Y.: *Q* value of anelastic S wave attenuation in Yunnan region, ACTA Seism. Sin., 20, 206–212, 2006.
Sun, X. D.: Some issues on estimation of strong ground motion field, Doctoral Thesis, Harbin Institute of Technology, Harbin, China, 132 pp., 2010.
Wang, G. X.: Research on the attenuation law of strong ground motion, Doctoral Thesis, Institute of Engineering Mechanics, CChina Earthquake Administration, Harbin, China, 150 pp., 2001.

NHESSD
3, 5297–5323, 2015

Wu, J. P., Ming, Y. H., and Wang, C. Y.: The *S* wave velocity structure beneath digital seismic stations of Yunnan province inferred from teleseismic receiver function modeling, Chinese J. Geophys.-Ch., 44, 228–237, 2001.

Xie, J., Ni, S. D., and Zeng, X. F.: 1D shear wave velocity structure of the shallow upper crust in central Sichuan Basin, Earthq. Res. Sichuan, 2, 20–24, 2012.

Zhang, Y. J., Qiao, H. Z., Cheng, W. Z., and Liu, J.: Attenuation characteristics of the media in Sichuan basin region, J. Seismol. Res., 30, 43–48, 2007.

NHESSD

3, 5297–5323, 2015

Table 1. Inverse results.

	$\Delta\sigma$ (MPa) 4–20	Q_0 90–400	η 0.2–0.8	R_1 (km) 50–100	R_2 (km) 100–150
Sichuan	85	155	0.6804	87	120
Yunnan	72	164	0.6647	83	122

NHESSD
3, 5297–5323, 2015

Table 2. Mean value and standard deviation of residuals.

Regions	M_w = 5.0		M_w = 6.0		M_w = 7.0	
	Mean value	Standard deviation	Mean value	Standard deviation	Mean value	Standard deviation
Sichuan	0.0832	0.3006	−0.0845	0.3320	−0.5262	0.2157
Yunnan	0.2097	0.5601	−0.0866	0.3061	0.0510	0.1610

NHESSD
3, 5297–5323, 2015

Table 3. Synthesized PGA and observed PGA at two rock stations.

Model	Maoxian station	Pixian station
1	411.0	120.7
2	290.5	156.3
3	285.0	123.3
4	340.9	109.9
5	265.4	140.8
6	284.8	152.5
7	330.9	141.5
8	295.2	137.3
9	312.6	153.4
10	234.3	142.3
11	338.3	123.9
12	244.6	149.8
13	305.6	133.6
14	315.5	143.9
15	349.7	102.6
16	310.8	135.2
17	369.0	160.4
18	337.6	128.7
19	285.8	122.1
20	314.4	131.8
21	418.3	124.0
22	247.8	124.0
23	357.8	109.9
24	262.0	145.8
25	343.1	113.2
26	284.3	108.5
27	301.8	128.5
28	284.3	181.4
29	336.1	123.2
30	222.6	138.6
Mean value of 30 models	309	134
Observed PGA on the EW direction	307	121
Observed PGA on the NS direction	302	142

NHESSD
3, 5297–5323, 2015

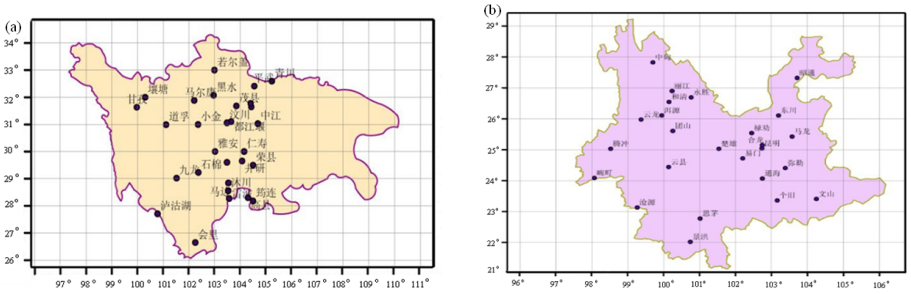

Figure 1. Seismological stations in **(a)** Sichuan region and **(b)** Yunnan region.

NHESSD
3, 5297–5323, 2015

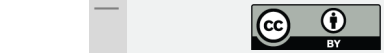

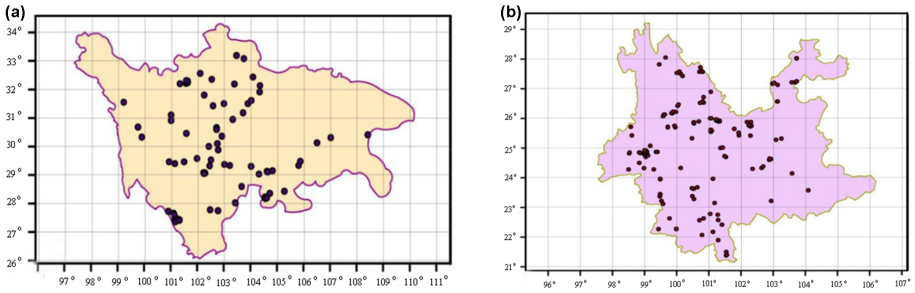

Figure 2. Small earthquakes in **(a)** Sichuan region and **(b)** Yunnan region.

NHESSD
3, 5297–5323, 2015

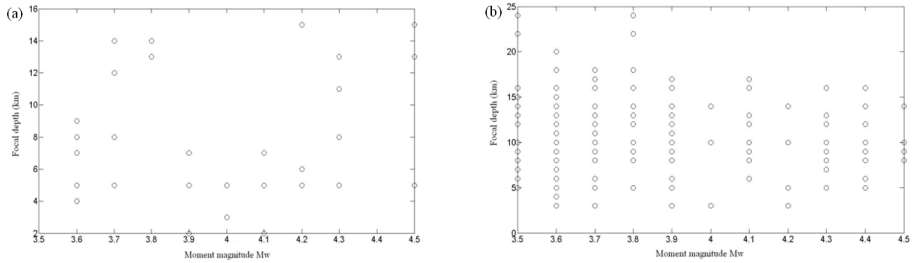

Figure 3. M_w-focal depth distribution of small earthquake records in **(a)** Sichuan region and **(b)** Yunnan region.

NHESSD
3, 5297–5323, 2015

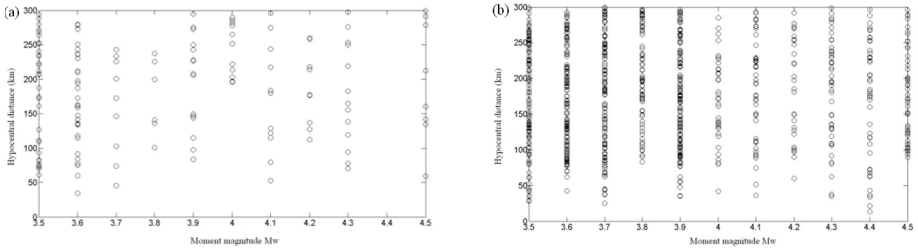

Figure 4. M_W-hypocentral distance distribution of small earthquake records in **(a)** Sichuan region and **(b)** Yunnan region.

NHESSD
3, 5297–5323, 2015

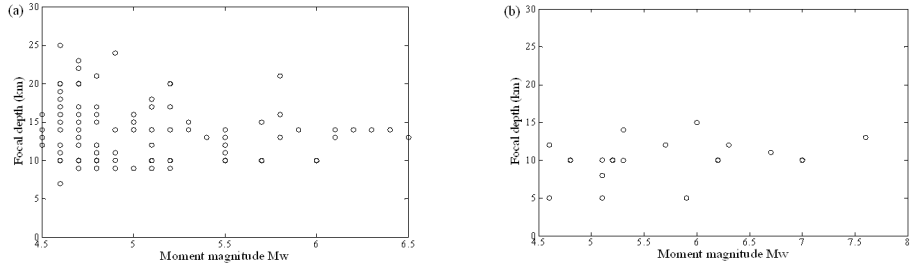

Figure 5. M_w-focal depth distribution of strong ground motion records in **(a)** Sichuan region and **(b)** Yunnan region.

NHESSD
3, 5297–5323, 2015

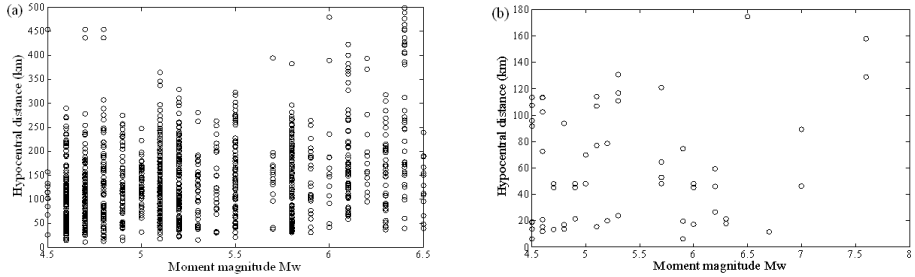

Figure 6. M_w-hypocentral distance distribution of strong ground motion records in **(a)** Sichuan region and **(b)** Yunnan region.

NHESSD
3, 5297–5323, 2015

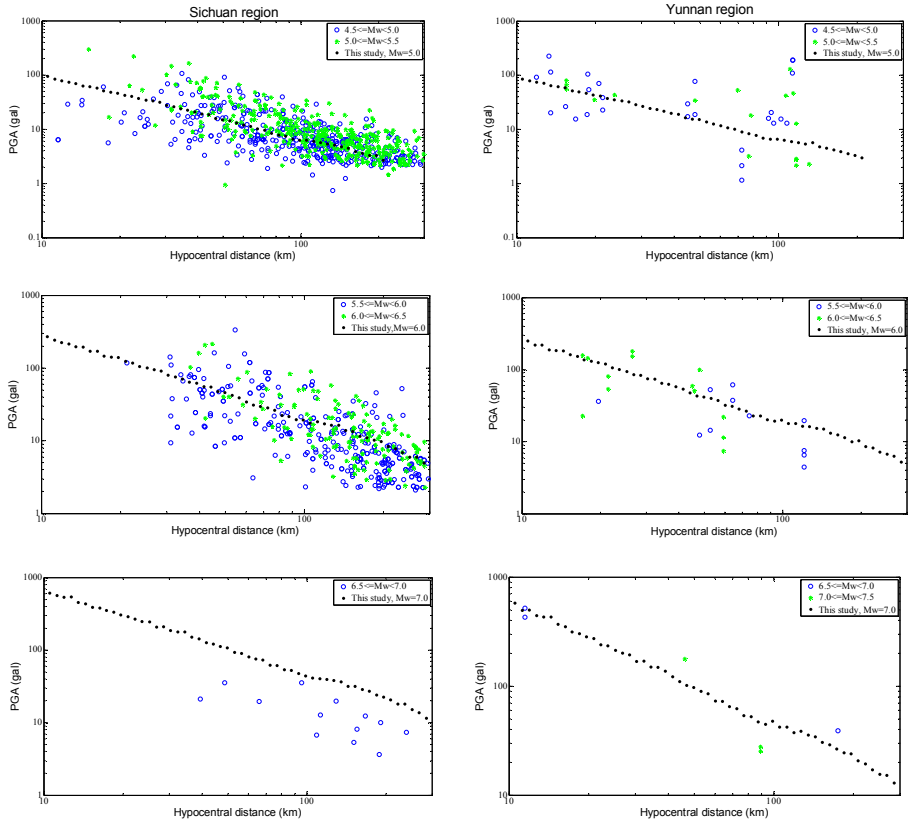

Figure 7. Compare the result with strong ground motion data in Sichuan region and Yunnan region.

NHESSD
3, 5297–5323, 2015

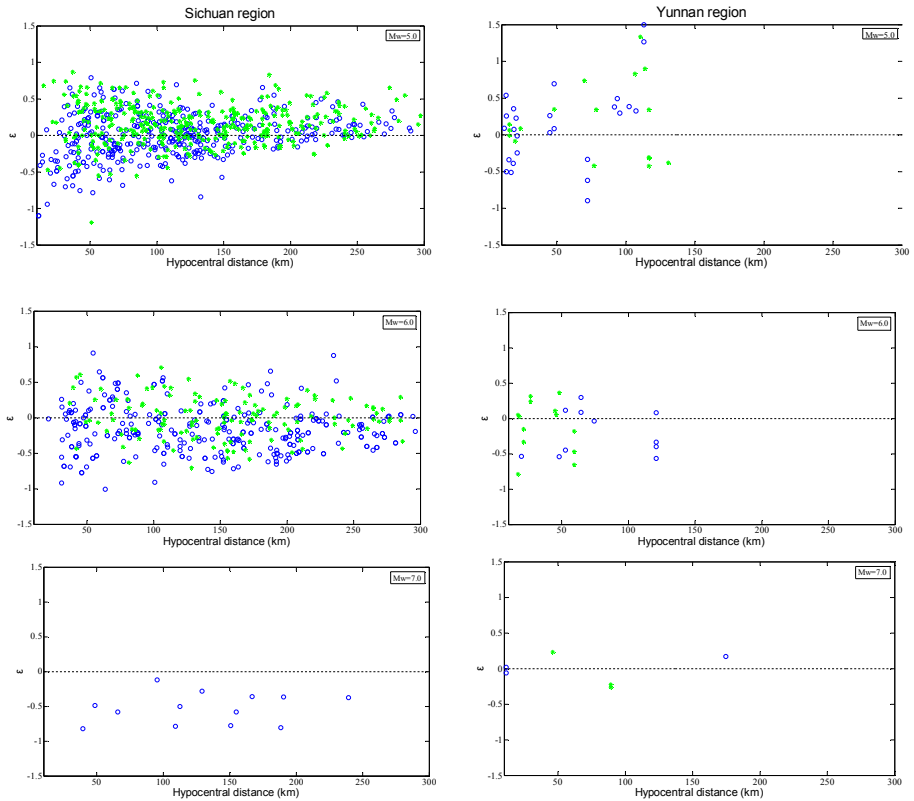

Figure 8. Residual distribution in Sichuan region and Yunnan region.

NHESSD
3, 5297–5323, 2015

Strong ground motion prediction for southwestern China from small earthquake records

Z. R. Tao et al.

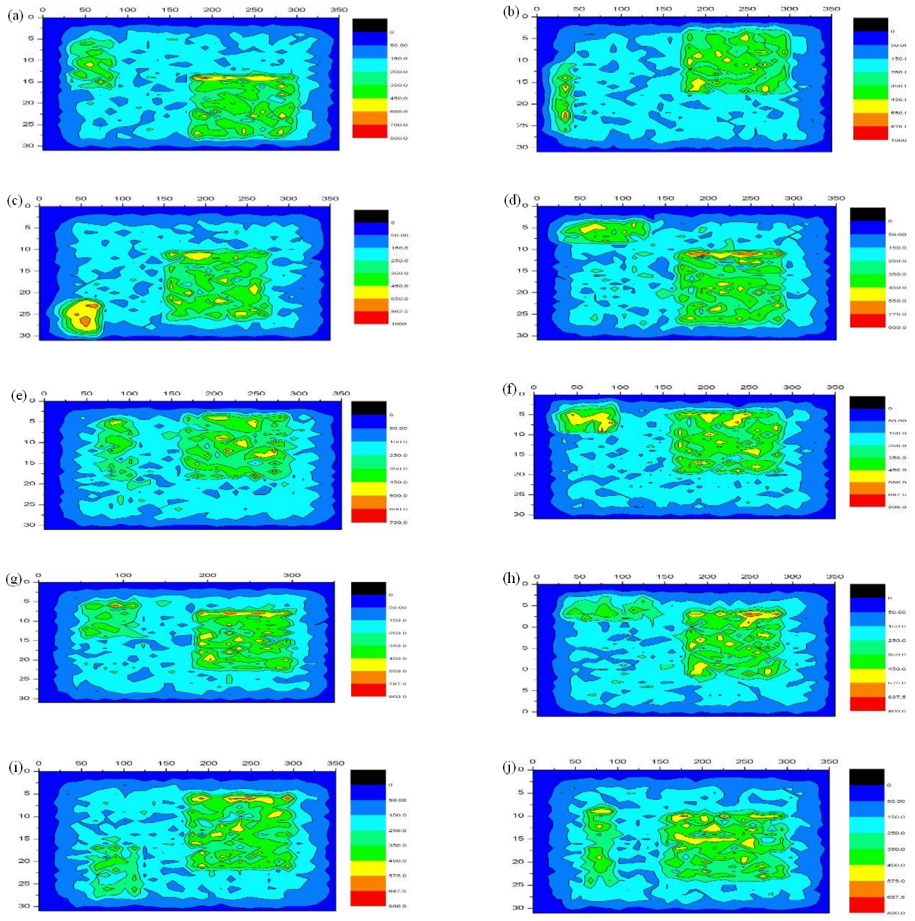

Figure 9. Ten hybrid source models in the case of Wenchuan Earthquake.

NHESSD
3, 5297–5323, 2015

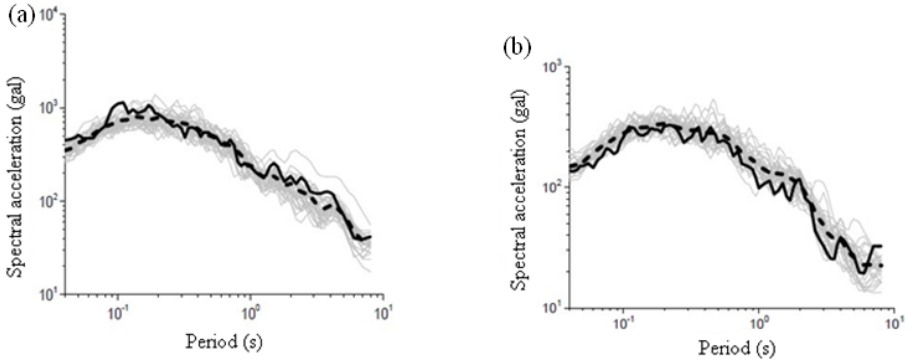

Figure 10. Response spectra from 30 hybrid source models for **(a)** Maoxian station and **(b)** Pixian station.

NHESSD
3, 5297–5323, 2015

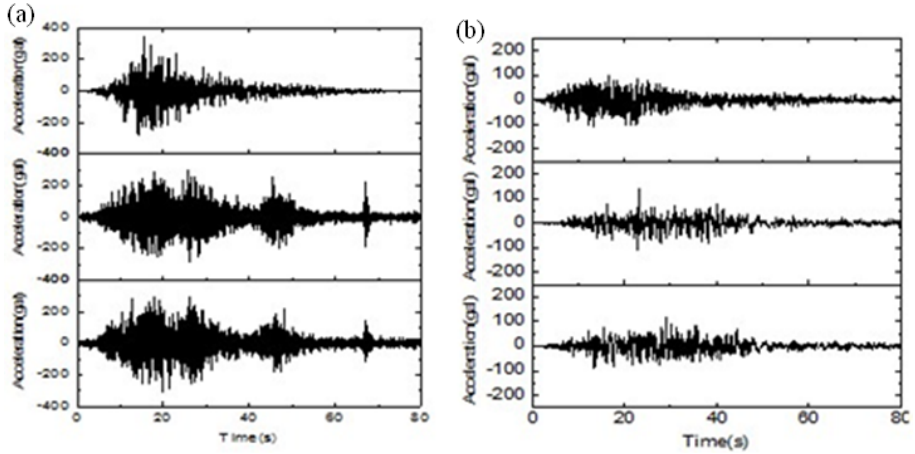

Figure 11. Comparison of time history for **(a)** Maoxian station and **(b)** Pixian station.

NHESSD
3, 5297–5323, 2015

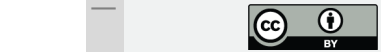

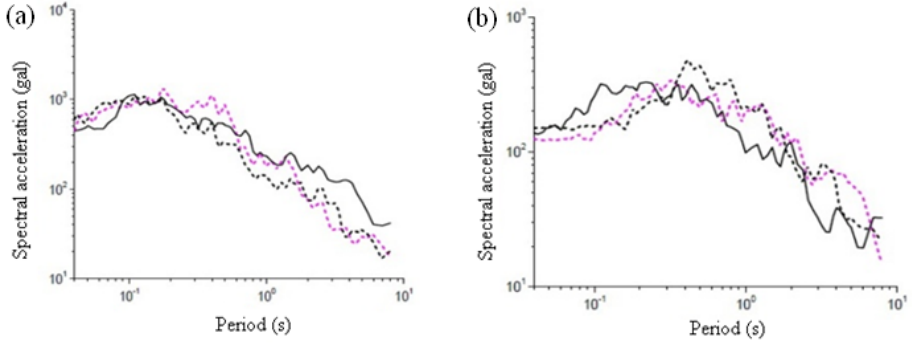

Figure 12. Comparison of response spectra for **(a)** Maoxian station and **(b)** Pixian station.

NHESSD
3, 5297–5323, 2015